Wideband, High-Density Circularly Polarized Array with Reduced Mutual Coupling and Enhanced Realized Gain

Zhiyuan Chen, *Student Member, IEEE*, Ming-Chun Tang, *Senior Member, IEEE*, Mei Li, *Member, IEEE*, Da Yi, *Member, IEEE*, Dongmei Mu, and Richard W. Ziolkowski, *Life Fellow*, *IEEE*

***Abstract* — A planar single-layer parasitic swastika-shaped structure, which serves as an effective isolator, is developed for mutual coupling reduction in wideband, high-density circularly polarized (CP) arrays. A closely spaced two-element CP antenna array demonstrates the efficacy of the approach. The currents induced by the CP coupling are effectively cancelled out when this isolator is integrated into it. The antenna elements are co-planar. They are arranged with a center-to-center distance of 0.4 λ_L (λ_L being the wavelength of the lower bound of the array's operational bandwidth) and have an extremely small edge-to-edge distance of ~ 0.024 λ_L. The parasitic element yields an increase of the isolation level between the antenna elements of more than 9.4 dB over the entire operational band, with a maximum improvement of 20.4 dB. Moreover, the antenna elements realize a modest maximum gain improvement of ~ 1.2 dB in the boresight direction over the same band. The overlapped impedance matching and 3-dB axial ratio (AR) bandwidths cover the range 1.7-2.7 GHz, a ~ 45% fractional bandwidth. A prototype was fabricated and measured; the measured results are in good agreement with their simulated values.**

***Index Terms* — Arrays, bandwidth, circular polarization, high-density arrays, mutual coupling**

I. Introduction

WIDEBAND circularly polarized (CP) antenna arrays have drawn enormous attention in modern wireless communication systems for their many inherent signal transmission advantages, including large channel capacity, anti-multipath interference, and polarization mismatch immunity [1]-[3]. In many practical engineering scenarios, e.g., in satellite and radar applications, the space between adjacent elements in an array is typically no more than a half-wavelength. This choice avoids grating lobes and facilitates the practical demands for wide-angle scanning, high resolution, high signal-to-noise ratio, and space-limited platforms [4]. Concomitantly, these high-density CP array configurations inescapably encounter strong mutual coupling between adjacent elements. These couplings generally deteriorate the array performance, e.g., worsen the impedance matching levels, distort the radiation patterns, reduce the radiation efficiencies, and degrade the CP purity [5], [6]. Consequently, it is highly desirable to construct an effective decoupling structure for wideband, high-density CP arrays that would significantly reduce the interelement couplings.

A variety of effective decoupling methods have been reported. They include utilizing distributed [7], [8] or lumped [9] decoupling networks behind the radiators. They also include locating electromagnetic band-gap (EBG) structures [10], defected ground structures (DGSs) [11], [12], neutralization lines [13], [14], metamaterial (MTM) structures [15]-[17], parasitic elements [18]-[21], artificial periodic metal strips [22], and polarization rotation walls [23] between the adjacent radiators. Furthermore, they include placing decoupling surfaces [24], [25] or frequency selective surfaces [26] above the radiators. However, these mutual coupling suppression methods have focused primarily on linearly polarized (LP) arrays [7]-[26].

Mutual coupling reduction for CP arrays is more challenging because of the additional requirement to maintain the quality of the axial ratio (AR) over the entire operational frequency band. Several recent efforts have reported methods to reduce mutual coupling effects in CP arrays. For example, a transmission-type FSS-based decoupling layer was placed on top of two closely spaced multiple-input, multiple-output (MIMO) CP antennas in [27]. A single-negative (SNG) metamaterial structure exhibiting a negative permittivity within the operational band was utilized in [28] for enhancing the isolation between the radiators of a two-element CP conformal array. Printed metallic strips were introduced in [29] between the closely spaced radiators of a two-element wideband MIMO CP microstrip antenna array to produce high isolation between them. A double-layer metamaterial absorber was designed to suppress

Manuscript received on Aug. 03, 2020, revised on July 06, 2021, and accepted on August 11, 2021.

This work was supported in part by the National Natural Science Foundation of China contract numbers 62031006, 62001065, and 61701052, in part by the Graduate Scientific Research and Innovation Foundation of Chongqing, China contract number CYS18062, in part by the Chongqing Natural Science Foundation contract number cstc2019jcyjjqX0004, and in part by the Australian Research Council grant number DP160102219. *(Corresponding author: Ming-Chun Tang.)*

Z. Chen, M.-C. Tang, M. Li, and D. Yi are with the Key Laboratory of Dependable Service Computing in Cyber Physical Society Ministry of Education, School of Microelectronics and Communication Engineering, Chongqing University, Chongqing, 400044, China and also with the State Key Laboratory of Power Transmission Equipment and System Security, Chongqing University, Chongqing, 400044, China. (E-mail: tangmingchun@cqu.edu.cn).

D. Mu is with the School of Electronic Engineering, Beijing University of Posts and Telecommunications, Beijing, 100876, China;

R. W. Ziolkowski is with the University of Technology Sydney, Global Big Data Technologies Centre, Ultimo NSW 2007, Australia (E-mail: Richard.Ziolkowski@uts. edu.au).

the mutual coupling of a CP four-element antenna array in [30]. A W-shaped parasitic strip was constructed in [31] as a decoupling tool for a two-element CP array with simultaneous transmitting and receiving functions. While these CP decoupling methods were shown to be effective, there are inherent drawbacks associated with each of them, which limit their widespread applications. In particular, these include relatively high profiles [27]; complex three-dimensional (3D) structures witnessing integration difficulties [28], [30]; degradations of the radiation gain performance [30]; and relatively narrow CP bandwidths [27]-[31].

A swastika-shaped parasitic structure printed on a planar single-layer dielectric superstrate is developed in this paper to significantly reduce the mutual coupling between the elements of a wideband, two-element high-density CP array. It is demonstrated that both an enhanced suppression of the mutual coupling (minimum ~ 9.4 dB) and a modest increase of the realized gain (maximum ~ 1.2 dB) are achieved when the parasitic structure is placed atop a closely spaced two-element CP antenna array whose fractional bandwidth is 45% around 2.2 GHz at the cost of only a 0.024 λ_L increase in the profile, where λ_L is the longest wavelength in the operating range. The wideband CP performance of the array is well maintained, a feature benefiting directly from the wideband CP characteristics of the swastika-shaped element itself. The measured results of a fabricated and tested prototype verified the effectiveness of the developed mutual coupling reduction structure.

In this paper, all of the numerical simulations and their optimizations were performed using the frequency domain, finite element-based ANSYS/ANSOFT High Frequency Structure Simulator (HFSS) [32].

II. Mutual Coupling Reduction Principles for CP Arrays

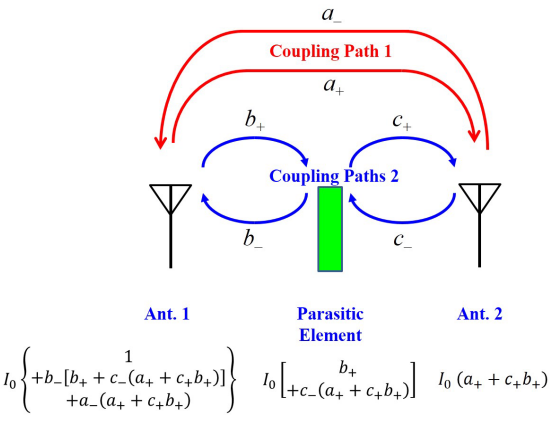

Fig. 1 Simplified schematic diagram of a two-element LP array with a parasitic element introduced to reduce the mutual coupling.

The concept of introducing a parasitic element to reduce the mutual coupling in a common two-element LP array is illustrated in Fig. 1. Ant. 1 is excited and Ant. 2 is passive and terminated with a 50 Ω matching load. The parasitic element is centered between these two antennas. The paths by which the radiated electromagnetic energy is coupled between the structures are identified. Coupling Path 1 is the space coupling between Ant. 1 and Ant. 2. The Coupling Paths 2 are the space couplings between the parasitic structure and those antennas.

Ant. 1 is excited with the current I_0. The currents b_+I_0 and a_+I_0 are then induced on the parasitic element and Ant. 2, respectively. Next, these induced currents lead to secondary couplings amongst the two antennas and the parasitic element. As a result, the currents on Ant. 1 consist of the excitation current I_0 and the secondary coupling currents $b_-[b_+ + c_-(a_+ + c_+b_+)]I_0$ from the parasitic element and $a_-(a_+ + c_+b_+)I_0$ from Ant. 2. The terms a_+, a_-, b_+, b_-, c_+, and c_+ represent the corresponding coupling coefficients. Similarly, the currents on Ant. 2 are the sum of a_+I_0 and $c_+b_+I_0$ arising from the couplings between Ant. 1 and the parasitic element, respectively. Finally, the currents on the parasitic element consist of b_+I_0 and $c_-(a_+ + c_+b_+)I_0$ arising from the couplings between Ant. 1 and Ant. 2, respectively.

It is theoretically anticipated that the coupling currents on Ant. 2 could be cancelled out entirely if the parasitic element were designed to induce out-of-phase currents on it with the same magnitude as the currents induced on it by the direct space path from Ant. 1. This feature would be achieved if

$$a_+I_0 + c_+b_+I_0 = 0 \tag{1}$$

Moreover, for an array of identical elements, the coupling coefficients b_+ and c_+ would be equal to each other. Thus, the coupling coefficients a_+, b_+, and c_+ can be expressed as $a_+ = |a_+|e^{j\varphi_1}$ and $b_+ = c_+ = |b_+|e^{j\varphi_2}$, where φ_1 and φ_2 represent the corresponding coupling phases, respectively. In order to also realize the coupling current cancellation on Ant. 2, one would adjust the parasitic structure so the associated coupling magnitudes and phases would satisfy the following conditions:

$$\begin{cases} |a_+| = |b_+|^2 \\ |\varphi_1 - 2\varphi_2| = \pi \end{cases} \tag{2}$$

Although the methodology of loading an array with parasitic structures is relatively simple and easy to implement, the reported structures, e.g., [18]-[20], are only suitable for LP arrays since the additional polarization characteristics introduced by the CP elements were not considered. Both the maintenance of the AR values and the CP purity levels are deemed critical factors for any mutual coupling reduction scheme developed for a CP array. Therefore, a parasitic decoupling structure having CP radiation characteristics is essential for mutual coupling reduction in a CP array.

In particular, if the CP array is assumed to lie in the *xy*-plane, the excitation current on CP Ant. 1 can be decomposed into two orthogonal currents with equal magnitudes and a 90° phase difference, e.g., an *x*-directed current I_0 and a *y*-directed current $I_0e^{\pm j\frac{\pi}{2}}$. Similarly, the *x*-directed component of the coupling currents on the parasitic element is then $[b_+ + c_-(a_+ + c_+b_+)]I_0$ and the *y*-directed component is

$[b'_+ + c'_-(a'_+ + c'_+ b'_+)]I_0 e^{\pm j\frac{\pi}{2}}$. Similarly, the x-directed component of the coupling currents on Ant. 2 is $(a_+ + c_+ b_+)I_0$ and the y-directed component is $(a'_+ + c'_+ b'_+)I_0 e^{\pm j\frac{\pi}{2}}$. In order to ensure that the parasitic element would operate in a CP state and would not deteriorate the CP purity of the array elements, the two discrete orthogonal currents on the parasitic structure should have equal amplitudes and a 90° phase difference. This requires

$$\begin{cases} a_+ = a'_+ = |a_+| e^{j\varphi_1} \\ b_+ = b'_+ = c_+ = c'_+ = c_- = c'_- = |b_+| e^{j\varphi_2} \end{cases} \tag{3}$$

A significant mutual coupling reduction is ensured if both orthogonal currents on CP Ant. 2 are cancelled out. This is achieved if

$$\begin{cases} (a_+ + c_+ b_+)I_0 = 0 \\ (a'_+ + c'_+ b'_+)I_0 e^{\pm j\frac{\pi}{2}} = 0 \end{cases} \tag{4}$$

In practice, one can at least achieve Eq. (2) to first order in the coupling coefficients. This decoupling methodology is verified in the analysis of all of the parasitic structures considered below.

III. Simple Decoupling Structure Integrated with a Wideband, Closely Spaced, Two-Element CP Array

The cross-dipole CP antenna reported in [1] was selected for our decoupling study. It is shown in Fig. 2. It has a wide operational bandwidth, a complete metal ground, and attractive radiation performance. Moreover, its radiating components substantially fill its aperture and, hence, they will be in close proximity to neighboring elements in any array formed with this antenna. Consequently, the CP antenna was a very challenging choice to demonstrate the effectiveness and universality of the decoupling methodology that we have developed.

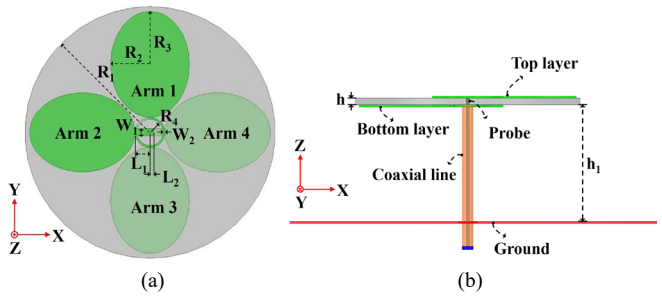

Fig. 2 Wide bandwidth, cross-dipole CP antenna configuration. (a) Top view. (b) Side view.

As shown in Fig. 2(a), two pairs of elliptical dipoles are printed on both sides of a Taconic CER-10 dielectric circular disk whose relative permittivity ε_r = 10.0, loss tangent tan δ = 0.0035, and thickness h = 1.0 mm. Arm 1 and Arm 2 lie on its upper surface; Arm 3 and Arm 4 lie on its bottom surface. The CP radiation performance is realized with a pair of ring-shaped phase-delay lines which connect the dipole Arms 1 and 2, and Arms 3 and 4, respectively, to form a 90° phase difference between the two orthogonal dipoles. The antenna is fed by a coaxial cable with its inner and outer conductors soldered to a pair of rectangular strips that are connected to the ring-shaped phase-delay lines. As shown in Fig. 2(b), a metal ground acts as a reflector. The radiating element is place directly above it at the height h_1 = 40.0 mm, where h_1 specifically represents the distance between the metal ground and the bottom of the radiating layer. The optimized design parameter values are given in Table I. With these values, the antenna radiates a left-hand circularly polarized (LHCP) field.

TABLE I. Design Parameters of the Wide Bandwidth LHCP Antenna (All Dimensions Are in Millimeters)

R_1 = 34.5	R_2 = 9.57	R_3 = 14.5	R_4 = 2.9	L_1 = 3.52
L_2 = 1.0	W_1 = 1.9	W_2 = 0.55	h_1 = 40.0	*null*

A. Two-element CP array

As shown in Fig. 3, the two-element array consists of two of the cross-dipole CP antennas, labeled NO. 1 and NO. 2. The array is configured with the center-to-center spacing D = 70.6 mm (0.4 λ_L). The metallic ground is circular with a radius of 125 mm. Only antenna NO. 1 is excited; antenna NO. 2 is passive and terminated in a 50-Ω load.

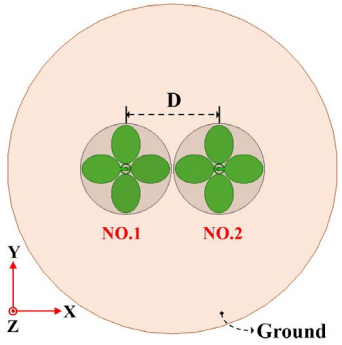

Fig. 3 Configuration of the closely spaced, wideband, two-element CP array.

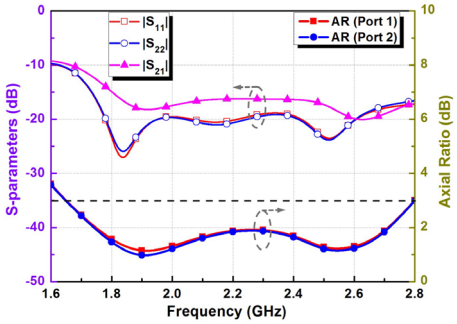

Fig. 4 Simulated S-parameters and AR results of the closely spaced, wideband, two-element CP array.

The simulated S-parameter and axial ratio (AR) results are shown in Fig. 4 when antenna No. 1 is active and No. 2 is passive and vice versa. It is observed that the CP antennas are

impedance well matched, i.e., $|S_{11}|$, $|S_{22}| < -10$ dB, over a wide bandwidth ranging from 1.7 to 2.7 GHz. As anticipated in [29]-[31], the mutual coupling level, i.e., $|S_{21}|$, is generally approaching -15 dB, and becomes higher, i.e., -10.9 dB, at 1.7 GHz. Fig. 5 depicts the surface current distributions at 1.9 GHz at four quarter-period time steps when antenna No. 1 is active and No. 2 is passive. The main current vector directions in each subplot are emphasized by black arrows for clear observation. When antenna NO. 1 operates in its LHCP state, strong coupling currents are induced on antenna NO. 2. The resulting mutual coupling level between the two antennas is high.

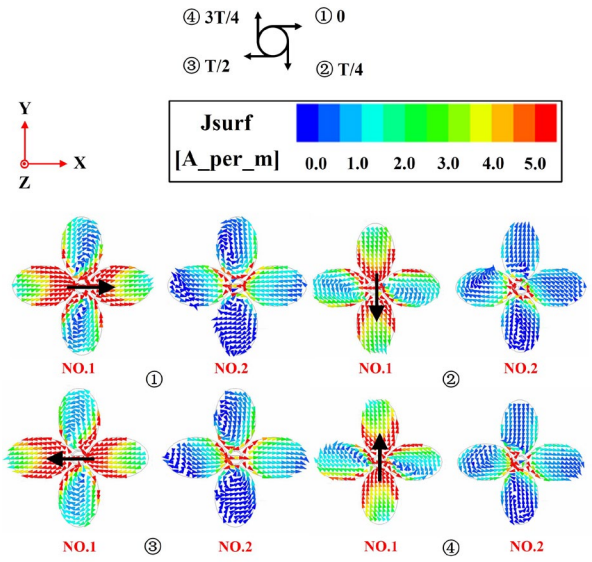

Fig. 5 Surface current distributions on both elements of the two-element CP array at four quarter-period time steps over one period at 1.9 GHz. The black arrows represent the maximum current direction.

B Two-element Array Loaded with Cross-Shaped Metallic Structure

Guided by the theoretical decoupling discussion, the two-element CP antenna array is augmented with a parasitic cross-shaped metallic structure. It is centered between the two elements and oriented along the *xy* coordinate axes as shown in Fig. 6(a). The width and length of both arms of the structure were optimized to be W_3 = 0.1 mm and L_3 = 105.0 mm, respectively. It is printed on the top surface of a low-cost FR4 substrate whose relative permittivity ε_r = 4.4, loss tangent tan δ = 0.02, and thickness h_4 = 1.0 mm. As shown in Fig. 6(b), this substrate is positioned above the radiating surfaces with an air-gap height of h_3 = 3.0 mm. Altering this height helps adjust the current magnitude and phase induced on the parasitic element. The distance between the radiating layer and the ground is set at h_2 = 36.0 mm to make the total height of the augmented array 41.0 mm, equal to that of the original CP array illustrated in Fig. 3.

The cross-shaped configuration of the decoupling structure facilitates the generation of orthogonal induced currents. Moreover, its relative size and orientation furnishes multiple induced current paths to realize the desired CP wideband decoupling operation. This CP feature is quite different from many of the recently reported decoupling methods for CP arrays that employ non-CP operating parasitic elements, e.g., metallic strips [29] and W-shaped parasitic strips [31].

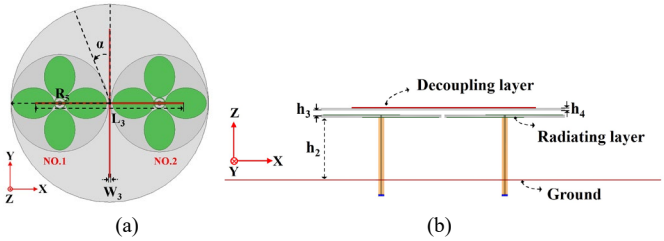

Fig. 6 Two-element CP array augmented with the cross-shaped parasitic decoupling structure. (a) Top view. (b) Side view.

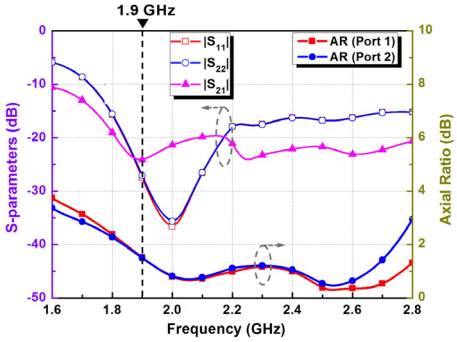

Fig. 7 Simulated results for the array loaded with the cross-shaped decoupling structure.

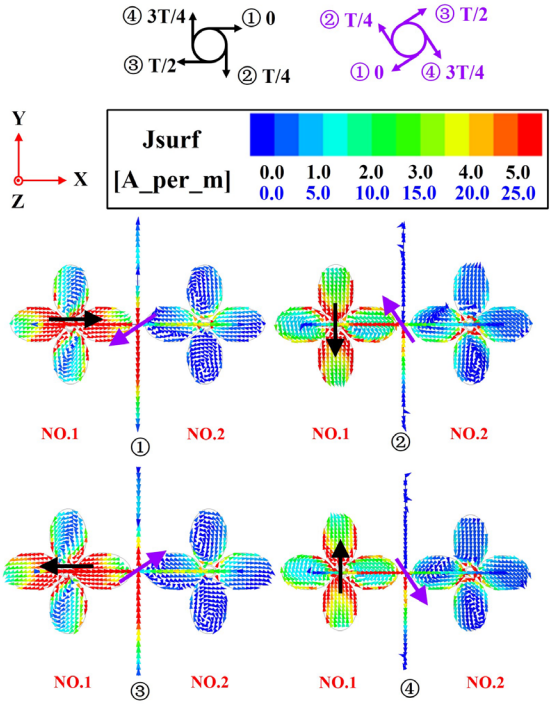

Fig. 8 Surface current distributions on the two-element CP array augmented with the parasitic cross-shaped decoupling structure at four quarter-period time steps over one period at 1.9 GHz. The vector directions of the currents on antenna NO. 1 and the cross-shaped decoupling structure are emphasized with the black and purple arrows, respectively

The simulated S-parameters and AR results of the augmented array corresponding to those in Fig. 4 are plotted in Fig. 7. In comparison, it is clearly observed that a decrease of

the $|S_{21}|$ values was achieved with the decoupling structure within the operational bandwidth, i.e., 1.7–2.7 GHz. Furthermore, the CP purity of the active antenna remains essentially unchanged over that bandwidth when antenna No. 1 is active, but a small variation occurs when antenna No. 2 is active at the upper portion of the operating band. This difference occurs because the individual radiating elements are not perfectly symmetric along the z direction, i.e., while the radiators are identical, two arms of each one lie on the top and on the bottom surfaces of the substrate.

The surface current distributions on the metallic pieces of the array when antenna No. 1 is active and antenna NO. 2 is passive are depicted in Fig. 8 at four quarter-period time steps over one period at the frequency 1.9 GHz, which corresponds to the point at which the mutual coupling decrease is maximum. The surface current vector directions on the active element and the decoupling structure are emphasized with black and purple arrows, respectively. The magnitude of the currents induced on the passive antenna NO. 2 is much lower in comparison to that in Fig. 5. The current directions also show that the parasitic decoupling structure operates in the LHCP state, which facilitates the maintenance of the CP purity.

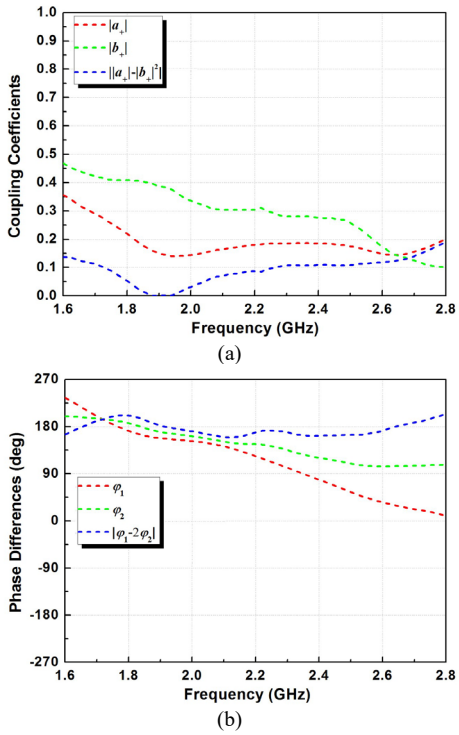

Fig. 9 Simulated coupling coefficient and current phase values of the two-element CP array augmented with the parasitic cross-shaped decoupling structure. (a) Magnitudes. (b) Phases.

The total current flowing through any directed curve segment of length l on a copper trace can be calculated as

$$i = \int_l \vec{J}_s \cdot (\vec{e}_n \times d\vec{l}) \tag{6}$$

where $\vec{J}_s$ represents the surface current density vector, $\vec{e}_n$ represents the unit vector perpendicular to the trace, and $d\vec{l}$ represents a small segment the directed curve. In this manner, the currents on each CP antenna were obtained by calculating this line integral across the feedlines, i.e., the two rectangular strips that connect the radiation patches and the coaxial cable. The total current on the parasitic decoupling structure can be obtained by adding the currents calculated along its two orthogonal directions. The normalized magnitudes of the currents induced by the fields radiated by the active antenna NO. 1 on the parasitic decoupling structure and on the passive antenna NO. 2 were calculated and normalized to those on the active antenna NO. 1 to obtain the coupling coefficients $|b_+|$ and $|a_+|$. The magnitudes and phases of these coefficients are plotted in Figs. 9(a) and 9(b), respectively. These results indicate that the decoupling structure effectively achieves the theoretical conditions in Eq. (2). Most of the currents are mutually cancelled, particularly in the lower frequency range where the difference $\left||a_+|-|b_+|^2\right|$ is -24.0 dB at 1.9 GHz. Moreover, the phase difference $|\varphi_1 - 2\varphi_2| \approx 180°$ across the entire operational band. On the whole, these results validate the decoupling analysis developed in Section II. In addition, it is noted that all of the design parameters, including those of the array and the cross-shaped metallic structure, were fixed at the same values as the ones presented in Table I to obtain the results shown in Fig. 9.

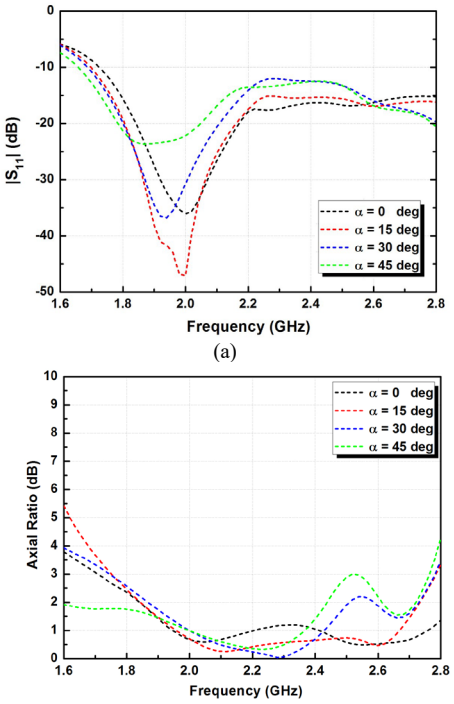

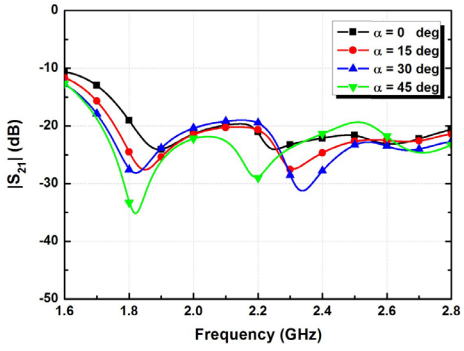

(c)

Fig. 10 Simulated (a) $|S_{11}|$, (b) AR, and (c) $|S_{21}|$ values as functions of the source frequency of the two-element CP array augmented when the cross-shaped decoupling structure is rotated by the angle α relative to the y-axis.

The effect of the rotation of the cross-shaped decoupling structure on the array performance was investigated. The rotation angle of the cross-shaped decoupling structure away from the y-axis in an anticlockwise direction is denoted as α. The simulated S-parameters and AR values of the augmented array when α varies from 0 to 45° with 15° increments while all of the other design parameters remain unchanged are plotted in Fig. 10. It is observed that the S-parameters and AR values vary only slightly as α increases. This outcome indicates that the array is basically insensitive to the orientation of the cross-shaped decoupling structure relative to it.

IV. Swastika-Shaped Decoupling Structure Integrated with a Wideband, Closely Spaced, Two-Element CP Array

While the cross-shaped decoupling structure was demonstrated to have a wide operating bandwidth and insensitivity to its orientation relative to the array elements, its size is much larger than the array elements. A swastika-shaped parasitic structure that is a simple modification of the cross-shaped one was developed to overcome that disadvantage. The configuration of the closely-spaced two-element CP array augmented with this parasitic element is illustrated in Fig. 11. The total height of the system is again maintained at 41.0 mm. The corresponding optimized design parameter values are listed in Table II.

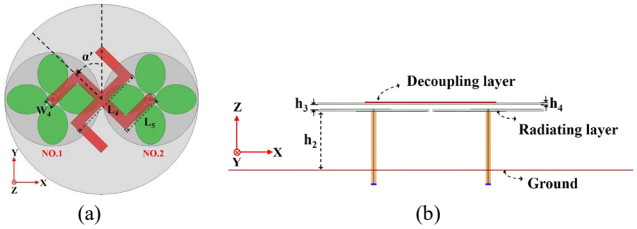

(a) (b)

Fig. 11 Closely-spaced two-element CP array augmented with the swastika-shaped parasitic structure. (a) Top view. (b) Side view.

Table II. Design Parameters of the Two-Element CP Array Augmented with the Swastika-Shaped Decoupling Structure (All Dimensions Are in Millimeters)

$R_1 = 34.5$	$R_2 = 10.86$	$R_3 = 14.5$	$R_4 = 3.6$	$R_5 = 70.0$
$L_1 = 4.2$	$L_2 = 1.0$	$L_4 = 56.0$	$L_5 = 31.0$	$W_1 = 2.0$
$W_2 = 0.55$	$W_4 = 7.0$	$h_2 = 36.0$	$h_3 = 3.0$	$h_4 = 1.0$

The simulated S-parameters and AR values of the swastika-augmented CP array are plotted in Fig. 12. The CP antennas are clearly well impedance matched within the range 1.7–2.7 GHz. In comparison to the original array, the isolation level is improved significantly, by more than 9.4 dB across the entire operational band. A maximum enhancement of 20.4 dB was achieved. Furthermore, the 3-dB AR bandwidths of the augmented array cover the entire bandwidth 1.7–2.7 GHz, i.e., the ~45% fractional bandwidth of the original array is maintained. This exceptional CP performance is attributed to the high isolation level between the CP antennas facilitated by the presence of the swastika-shaped decoupling structure.

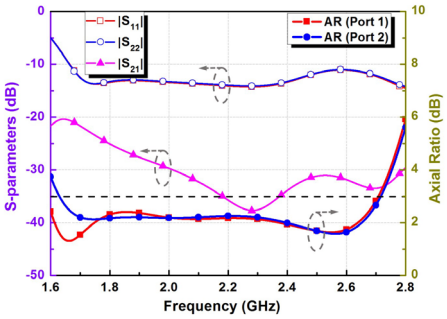

Fig. 12 Simulated S-parameter and AR values as functions of the source frequency of the swastika-augmented closely-spaced two-element CP array.

The surface current distributions on the metallic pieces of the swastika-augmented closely-spaced two-element CP array are presented in Fig. 13 at four quarter-period time steps over one period at three frequencies: 1.7, 2.2, and 2.7 GHz when antenna NO. 1 is active and antenna NO. 2 is passive. The vector directions of the surface currents on the excited antenna NO. 1 and the parasitic element are again emphasized by black and purple arrows, respectively. It is very clear that when antenna NO. 1 operates in the LHCP state, the coupling currents on antenna NO. 2 are very weak. Again, this outcome is attributed to the approximate cancellation of the induced currents associated with the coupling path 1 and coupling paths 2.

It is emphasized that the swastika-shaped structure provides two orthogonal paths for the induced currents that are instrumental in the cancellation of the CP coupling fields. In fact, the swastika-shaped structure operates as a parasitic CP radiator once the initially radiated CP fields induce the corresponding currents on it. It not only acts as a decoupling structure, but also as a parasitic LHCP radiator that contributes to the gain of the array. Comparing the current distributions in Figs. 13(a)-13(c), it is obvious that their vector directions on the swastika-shaped decoupling structure vary in lock-step with the change of the excitation phase of antenna NO. 1 in its LHCP state.

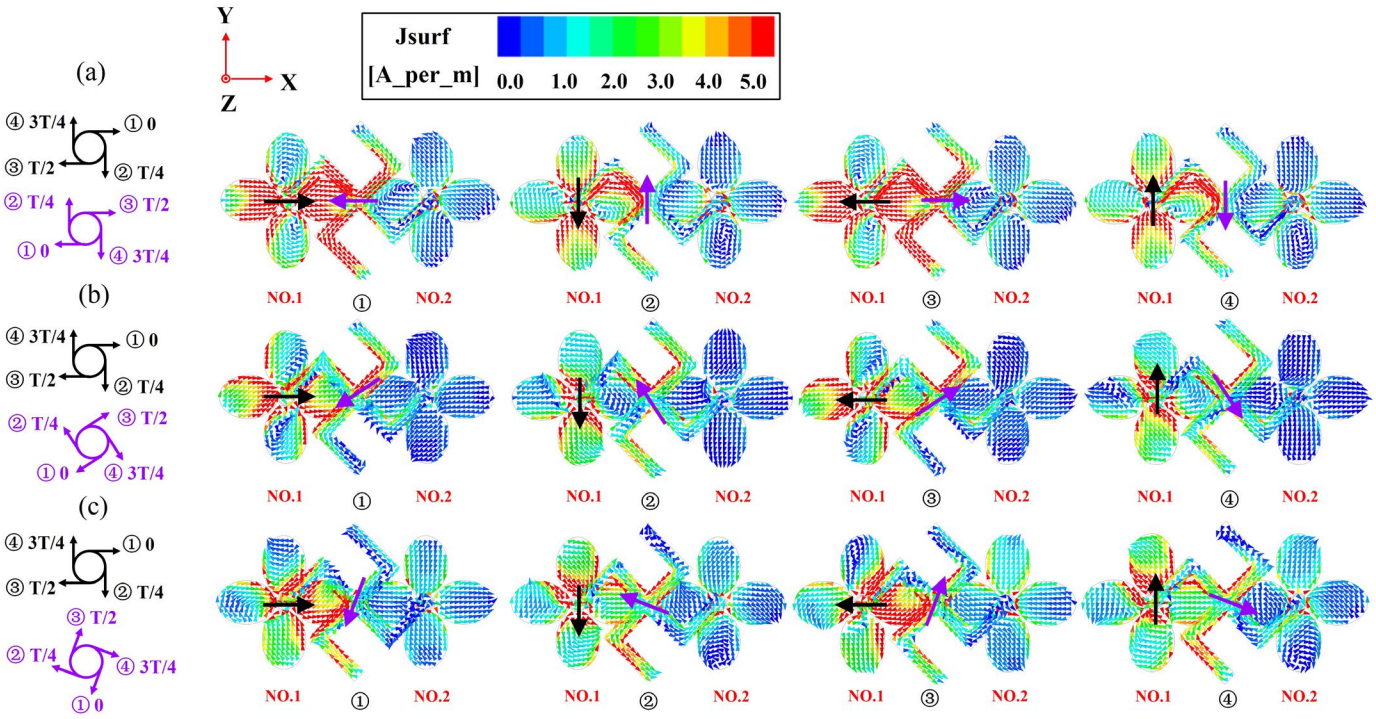

Fig. 13 Surface current distributions on the closely-spaced two-element CP array augmented with the parasitic swastika-shaped structure at four quarter-period time steps over one period when only antenna No. 1 is excited at the three frequencies: (a) 1.7, (b) 2.2, and (c) 2.7 GHz. The vector directions of the currents on antenna NO. 1 and the swastika-shaped decoupling structure are emphasized with the black and purple arrows, respectively.

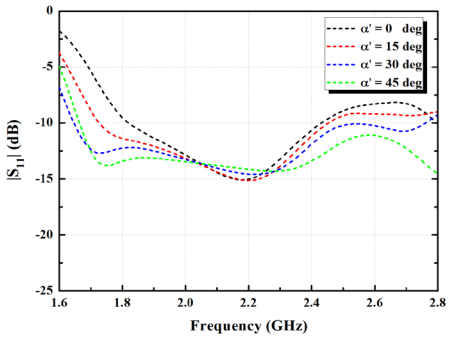

(a)

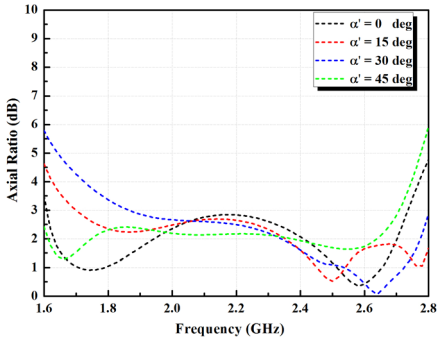

(b)

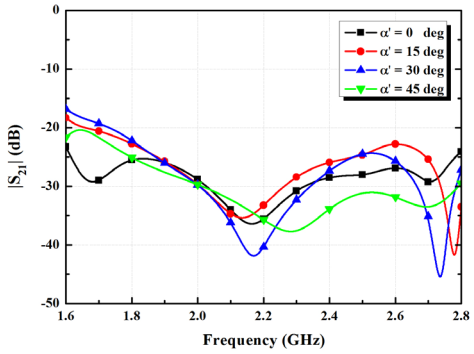

(c)

Fig. 14 Simulated (a) $|S_{11}|$, (b) AR, and (c) $|S_{21}|$ values as functions of the source frequency when the swastika-shaped decoupling structure is rotated by the angle α with respect to the closely-spaced two-element CP array.

The effect of the orientation of the swastika-shaped decoupling structure on the performance of the closely-spaced two-element CP array was also investigated. The rotation angle, α', was again taken to be the angle away from the y-axis. The simulated S-parameters and AR values as functions of the source frequency when α' was varied from 0 to 45° with 15° increments while all of the other design parameters remain unchanged are plotted in Fig. 14. It is apparent that the reflection coefficient for each CP antenna is more sensitive to the rotation angle α' in comparison to the cross-shaped decoupling structure augmented version. On the other hand, the isolation levels, $|S_{21}|$, remain high and the AR values only vary a slight amount. In particular, the impedance matching of the CP antennas improves as α' varies from 0 to 45°. When $\alpha' =$ 45°, the optimal array performance is attained.

The effect that the air-gap height, h_3, has on the decoupling performance was also investigated numerically. It is one of the key design parameters of the swastika-augmented CP array. The simulated S-parameters and AR values as functions of the source frequency when h_3 varies from 1.0 to 7.0 mm with 2.0 mm increments while all of the other design parameters remain unchanged are plotted in Fig. 15. Clearly, when h_3 changes, the impedance match and AR values are significantly impacted in the lower frequency range of the operating band as is shown in Figs. 15 (a) and 15(b). On the other hand, as observed in Fig. 15(c), the coupling level, i.e., the value of $|S_{21}|$, increase particularly in the higher portion of the operating band when h_3 increases.

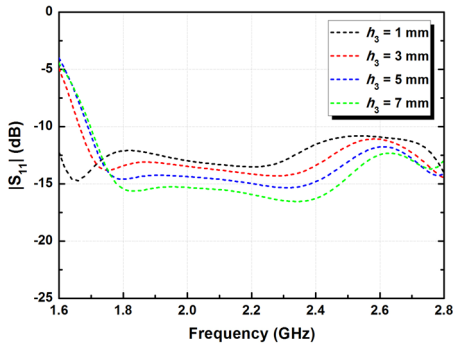

(a)

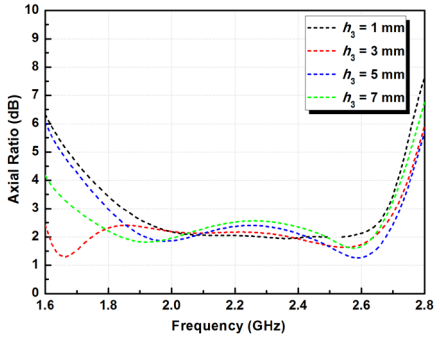

(b)

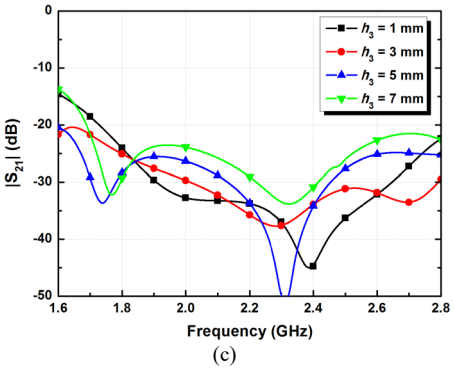

(c)

Fig. 15 Simulated (a) $|S_{11}|$, (b) AR, and (c) $|S_{21}|$ values as functions of the source frequency of the closely-spaced two-element CP array augmented with the parasitic swastika-shaped structure for different h_3 values.

All of these simulation results have demonstrated that the swastika-shaped parasitic structure serves as a very effective wideband, CP decoupling element. The design is compact even relative to the closely-spaced two-element CP array. To further demonstrate its efficacy, both the 3-element and 4-element CP arrays augmented with the swastika-shaped decoupling elements shown in Fig. 16 were simulated. They both exhibited a 42% broad fractional bandwidth from 1.7 to 2.6 GHz. The port isolation level with the swastika-shaped elements being present was more than 28 dB across this operational band in both cases. The peak isolation enhancement over the same arrays without the decoupling elements was 13 and 33 dB in the 3- and 4-element cases, respectively. These simulation results confirm the effectiveness of the swastika-shaped element decoupling approach even for larger CP arrays.

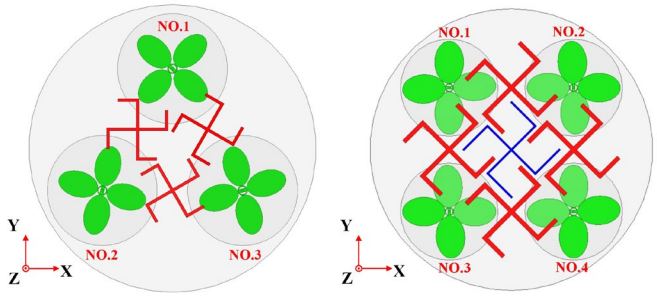

(a) (b)

Fig. 16 Closely-spaced (a) three- and (b) four-element CP arrays augmented with swastika-shaped parasitic decoupling elements.

Note that similar swastika-shaped elements have also been proven effective as chiral metamaterial structures [33-36], frequency selective surfaces [37], [38], microwave absorbers [39] and antenna array decoupling tools [40]. However, in their practical applications, those swastika-shaped structures were required to be in periodic arrangements [33]–[38] and/or in one-by-one connection arrangements between multiple elements [39], [40] to achieve their specific properties. In contrast, the single swastika-shaped element in our decoupling approach operates as a CP radiator that induces secondary coupling currents on the adjacent CP radiators to suppress the coupling effects.

V. Experimental Results and Discussion

The optimized, closely-spaced two-element wideband CP array augmented with the developed swastika-shaped decoupling structure was fabricated and experimentally studied. Photographs of the decoupling structure and the CP array prototype are shown in Fig. 17. The reflection coefficients for each CP antenna and the mutual coupling level between them were measured using an Agilent E8361A PNA vector network analyzer (VNA). The measured results are given in Fig. 18 and are compared to their simulated values, as well as to those of the original wide-bandwidth CP array. The input impedance is well-matched to the source over the entire predicted ~45% fractional operational bandwidth from 1.7–2.7 GHz. Even with the inter-element (edge-to-edge) spacing between the two radiating elements being 0.4 λ_L (0.024 λ_L), the measured isolation level between them is better than 25.0 dB across that bandwidth. The minimum (maximum) isolation enhancement ~12.0 dB (~31.0 dB) was achieved in comparison to the original array. Furthermore, when compared with the two-element array augmented with the cross-shaped decoupling structure, swastika version achieved higher isolation levels with a more compact size. Good agreement between the simulated and measured values was obtained in

general. The typical unavoidable fabrication tolerance and measurement errors led to the observed small discrepancies. The associated scattering losses also contribute the measured isolation levels being slightly better than their simulated ones.

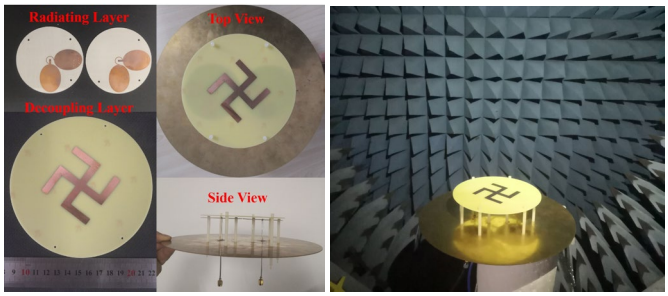

(a) (b)

Fig. 17 Fabricated prototype of the developed closely-spaced two-element CP array augmented with the parasitic swastika-shaped structure. (a) The decoupling structure and radiating elements alone and with them assembled into the array. (b) Antenna under test (AUT) in the anechoic chamber.

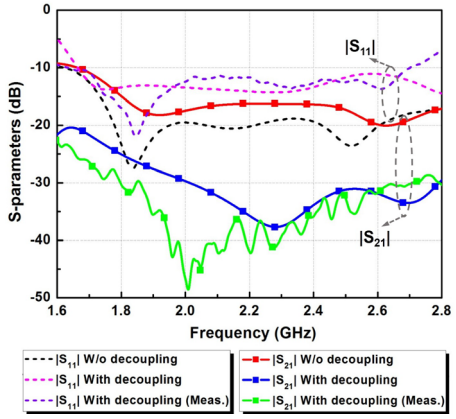

Fig. 18 Simulated and measured reflection coefficients and isolation levels of the closely-spaced two-element CP array with and without the swastika-shaped parasitic decoupling structure, when antenna NO. 1 is active and antenna NO. 2 is passive, as functions of the source frequency.

The far-field radiation performance of the prototype was measured using a SATIMO passive measurement system in a chamber at the University of Electronic Science and Technology of China (UESTC). The simulated and measured AR curves when antenna NO. 1 of the array was excited with and without the parasitic swastika-shaped structure being present are compared in Fig. 19. The measured results are again very consistent with their simulated values. All of the measured results confirm that the swastika-shaped isolator effectively reduces the coupling between the radiating elements in this high-density array while maintaining its wideband CP performance.

The simulated and measured far-field radiation patterns of the closely-spaced two-element CP array with and without the swastika-shaped parasitic structure when only antenna NO. 1 is active are shown in Fig. 20. They are presented for the frequencies 1.8, 2.2, and 2.5 GHz to illustrate the stability of the pattern over the wide operating bandwidth. The simulated peak realized gain values of the CP array with (without) the coupling structure are 7.1 dBi (6.97 dBi), 7.31 dBi (6.26 dBi), and 6.18 dBi (4.96 dBi), respectively, at 1.8, 2.2, and 2.5 GHz. The corresponding simulated half-power beam-width (HPBW) in the *zox*-plane cover the range from -47° to 45° (from -15° to 47°), from -44° to 38° (from -45° to 54°), and from -46° to 33° (from -35° to 57°). The associated HPBW in the *yoz*-plane cover the range from -25° to 40° (from -36° to 33°), from -32° to 41° (from -44° to 41°), and from -48° to 49° (from -58° to 51°). One observes that the radiation patterns of the array with the decoupling structure are more symmetric with higher gain values, i.e., a modest maximum gain improvement of ~1.2 dB, as compared to those of the original array without it. Moreover, the RHCP radiation patterns of the arrays with and without the developed decoupling structure are also plotted and compared in Fig. 20. It is shown that the decoupling structure has little influence on the cross-polar level of the array element.

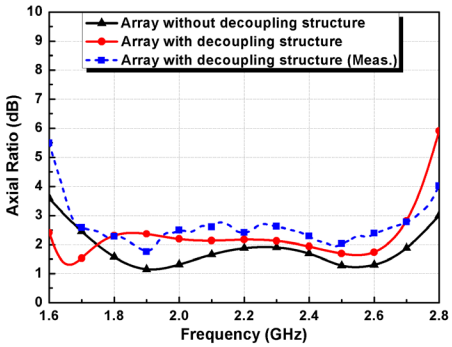

Fig. 19 Simulated and measured AR values of the close-spaced two-element CP array with and without the swastika-shaped parasitic decoupling structure, when antenna NO. 1 is active and antenna NO. 2 is passive, as functions of the source frequency.

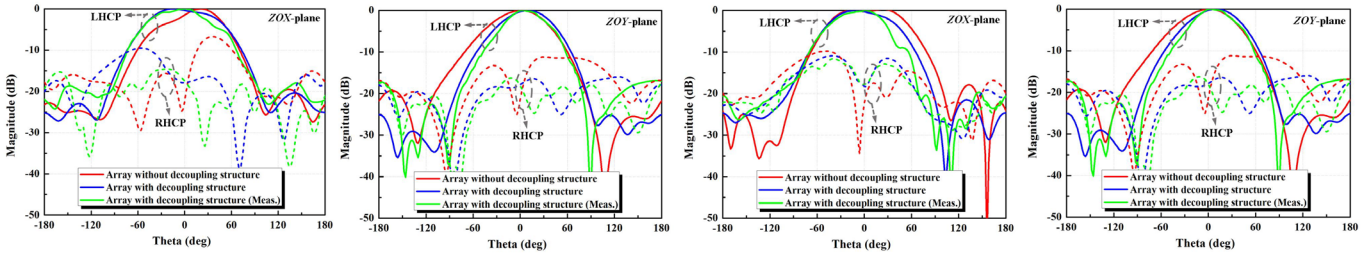

(a) (b)

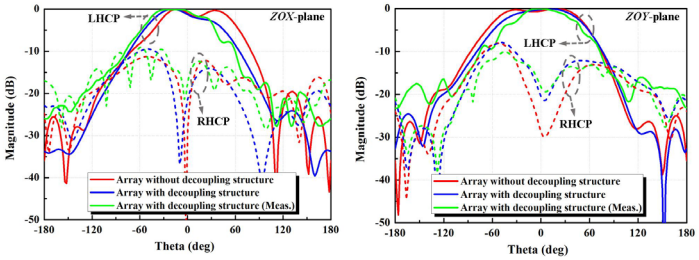

(c)

Fig. 20 Simulated and measured LHCP and RHCP radiation patterns of the close-spaced two-element CP array with and without the parasitic swastika-shaped structure at three different frequencies in the operating bandwidth when only antenna NO. 1 was excited. (a) @ 1.8 GHz. (b) @ 2.2 GHz. (c) @ 2.5 GHz.

TABLE III. PERFORMANCE COMPARISON WITH RECENTLY REPORTED METHODS FOR THE CP ARRAYS

Ref.	Element Separation (λ_0)	Edge-to-edge Distance (λ_0)	Overlapped AR & Operational FBW (%)	Gain Enhancement Level (dB)	Minimum Decoupling Level (dB)	Decoupling Structure Configuration
[27]	0.5	0.18	3.9	NA	~7.0	Planar
[28]	~0.7	~0.35	< 20.0	1.0	~3.0	3-D
[29]	~0.6	0.3	23.0	NA	~5.0	Planar
[30]	0.4	0.28	1.9	-1.2	8.0	3-D
[31]	0.18	0.033	0.97	1.1	15.0	Planar
This Work	0.4	0.024	45.0	1.2	9.4	Planar

The simulated and measured peak LHCP realized gain values are compared in Fig. 21. The simulated (measured) realized gain values at the frequencies 1.8, 2.2, and 2.5 GHz are 7.1 dBi (7.15 dBi), 7.31 dBi (7.25 dBi) and 6.18 dBi (6.38 dBi), respectively. The corresponding simulated (measured) HPBW values in the *zox*-plane are 92° (79°), 82° (69°), and 79° (80°). Those in the *yoz*-plane are 65° (56°), 73° (58°), and 97° (77°). Notice that the broadside realized gain values in the higher frequency portion of the bandwidth are enhanced more than those in the lower one. This effect arises because the half-power beam-widths become narrower in that higher range once the decoupling element is present. Finally, the simulated (measured) overall efficiency values of the swastika-augmented CP array are all above 90% (80%) over the entire operating bandwidth.

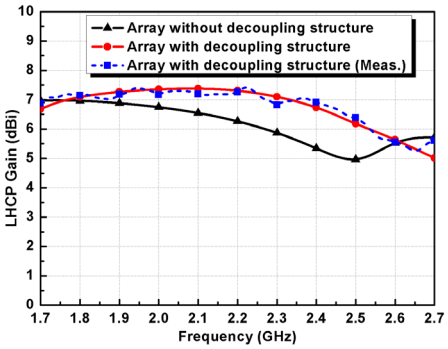

Fig. 21 Simulated and measured LHCP realized gain values of the close-spaced two-element CP array with and without the parasitic swastika-shaped structure.

As was demonstrated, the mutual coupling reduction in the prototype high-density CP array augmented with the swastika-shaped parasitic decoupling element led to enhanced element isolation, a realized gain improvement and radiation pattern stability while maintaining its original wide operating bandwidth, CP purity and high radiation efficiency. Table III compares these performance characteristics with CP arrays augmented with other types of decoupling structures. For a fair comparison, it includes the element separations, edge-to-edge distances, overlapped AR and operational bandwidths, gain enhancement levels, minimum decoupling levels, and decoupling structure configurations. It clearly shows that the optimized prototype not only achieves the largest fractional bandwidth with the smallest edge-to-edge distance, but it also has symmetric radiation patterns with improved peak gain values while having the advantages of a simple, planar, and easy-to-integrate decoupling structure configuration.

We note that our studies suggest that rotationally symmetric parasitic resonators that allow the radiators of a CP array to induce orthogonal currents on them with a 90° phase difference would also serve as effective decoupling elements. For instance, a crossed S-shaped structure is also an effective CP decoupling element. The reason that we utilized the swastika-shaped structure is that it possesses a relatively compact size, which makes it more suitable for the high-density CP arrays that were being considered. We also note that our CP decoupling approach can be readily extended to dual-linearly-polarized arrays such as those serving as commercial base-station antennas [17].

VI. CONCLUSION

In this paper, both planar cross-shaped and compact swastika-shaped parasitic decoupling structures were developed and integrated with a very wide bandwidth, closely-spaced two-element CP array. A theoretical analysis of a general parasitic decoupling structure was presented to understand the coupling paths and the concept that the currents induced on the parasitic can be manipulated to mitigate the coupling and, hence, increase the isolation levels between the radiating elements of an array. The analysis was confirmed with the cross-shaped case. The swastika-shaped parasitic was developed because the cross-shaped element was not compact relative to the size of the selected proof-of-concept array. It was demonstrated that a wide bandwidth, closely-spaced

two-element CP array augmented with the swastika-shaped parasitic structure has significantly improved isolation levels between the radiating elements, improved peak realized gain values, and stable radiation patterns while maintaining the wide bandwidth, CP purity, and high radiation efficiency of the original array. A prototype of the optimized swastika-augmented CP array was fabricated and measured. The experimental results, in good agreement with their simulated values, confirmed the efficacy of the developed CP decoupling structure. Benefitting from its simple, planar and low cost configuration, the innovative swastika-shaped decoupling parasitic structure is quite suitable for implementation in other high-density CP arrays. As a very effective isolator, it has potential applicability to many multi-function, wide-angle scanning phased, and MIMO arrays employed in compact mobile platforms as well as to densely-packed multi-band base station arrays that are under consideration for 5G and beyond wireless systems.

REFERENCES

[1] L. Zhang, S. Gao, Q. Luo, P. R. Young, Q. Li, Y.-L. Geng, and R. A. Abd-Alhameed, "Single-feed ultra-wideband circularly polarized antenna with enhanced front-to-back ratio," *IEEE Trans. Antennas Propag.*, vol. 64, no. 1, pp. 355-360, Jan. 2016.

[2] T. Nguyen, H. Tran, and N. Nguyen-Trong, "A wideband dual-cavity-backed circularly polarized crossed dipole antenna," *IEEE Antennas Wireless Propag. Lett.,* vol. 16, pp. 3135-3138, 2017.

[3] W. Yang, Y. Pan, S. Zheng, and P. Hu, "A low-profile wideband circularly polarized crossed-dipole antenna," *IEEE Antennas Wireless Propag. Lett.,* vol. 16, pp. 2126-2129, 2017.

[4] M. J. Al-Hasan, T. A. Denidni, and A. R. Sebak, "Millimeter-wave compact EBG structure for mutual coupling reduction applications," *IEEE Trans. Antennas Propag.*, vol. 63, no. 2, pp. 823–828, Feb. 2015.

[5] K. Vishvaksenan, K. Mithra, R. Kalaiarasan, and K. Raj, "Mutual coupling reduction in microstrip patch antenna arrays using parallel coupled-line resonators," *IEEE Antennas Wireless Propag. Lett.,* vol. 16, pp. 2146-2149, 2017.

[6] K. L. Chung and S. Kharkovsky, "Mutual coupling reduction and gain enhancement using angular offset elements in circularly polarized patch array," *IEEE Antennas Wireless Propag. Lett.,* vol. 12, pp. 1122-1124, 2013.

[7] K.-C. Lin, C.-H. Wu, C.-H. Lai, and T.-G. Ma, "Novel dual-band decoupling network for two-element closely spaced array using synthesized microstrip lines," *IEEE Trans. Antennas Propag.*, vol. 60, no. 11, pp. 5118-5128, Nov. 2012.

[8] X.-J. Zou, G.-M. Wang, Y.-W. Wang, and H.-P. Li, "An efficient decoupling network between feeding points for multielement linear arrays," *IEEE Trans. Antennas Propag.*, vol. 67, no. 5, pp. 3101-3108, May 2019.

[9] C.-H. Wu, C.-L. Chiu, and T.-G. Ma, "Very compact fully lumped decoupling network for a coupled two-element array," *IEEE Antennas Wireless Propag. Lett.*, vol. 15, pp. 158–161, 2016.

[10] F. Yang and Y. Rahmat-Samii, "Microstrip antennas integrated with electromagnetic band-gap (EBG) structures: A low mutual coupling design for array applications," *IEEE Trans. Antennas Propag.*, vol. 51, no. 10, pp. 2936-2946, Oct. 2003.

[11] S. Xiao, M.-C. Tang, Y.-Y. Bai, S. Gao, and B.-Z. Wang, "Mutual coupling suppression in microstrip array using defected ground structure," *IET Microw. Antennas Propag.*, vol. 5, no. 12, pp. 1488 - 1494, Sep. 2011.

[12] K. Wei, J.-Y. Li, L. Wang, Z.-J. Xing, and R. Xu, "Mutual coupling reduction by novel fractal defected ground structure bandgap filter," *IEEE Trans. Antennas Propag.*, vol. 64, no. 10, pp. 4328-4335, Oct. 2016.

[13] A. Diallo, C. Luxey, P. Thuc, R. Staraj, and G. Kossiavas, "Study and reduction of the mutual coupling between two mobile phone PIFAs operating in the DCS1800 and UMTS bands," *IEEE Trans. Antennas Propag.*, vol. 54, no. 11, pp. 3063-3074, Nov. 2006.

[14] S. Zhang and G. F. Pedersen, "Mutual coupling reduction for UWB MIMO antennas with a wideband neutralization line," *IEEE Antennas Wirel. Propag. Lett.*, vol. 15, pp. 166-169, 2016.

[15] M.-C. Tang, S. Xiao, B.-Z. Wang, J. Guan, and T. Deng, "Improved performance of a microstrip phased array using broadband and ultra- low-loss metamaterial slabs," *IEEE Antennas Propag. Mag.*, vol. 53, no. 6, pp. 31 - 41, Dec. 2011.

[16] A. Jafargholi, A. Jafargholi, and J. H. Choi, "Mutual coupling reduction in an array of patch antennas using CLL metamaterial superstrate for MIMO applications," *IEEE Trans. Antennas Propag.*, vol. 67, no. 1, pp. 179-189, Jan. 2019.

[17] M.-C. Tang, Z. Chen, H. Wang, M. Li, B. Luo, J. Wang, Z. Shi, and R. W. Ziolkowski, "Mutual coupling reduction using meta-structures for wideband, dual-polarized, and high-density patch arrays," *IEEE Trans. Antennas Propag.*, vol. 65, no. 8, pp. 3986-3998, Aug. 2017.

[18] A. C. K. Mak, C. R. Rowell, and R. D. Murch, "Isolation enhancement between two closely packed antennas," *IEEE Trans. Antennas Propag.*, vol. 56, no. 11, pp. 3411-3419, Nov. 2008.

[19] Ó. Quevedo-Teruel, Z. Sipus, and E. Rajo-Iglesias, "Characterization and reduction of mutual coupling between stacked patches," *IEEE Trans. Antennas Propag.*, vol. 59, no. 3, pp. 1031-1036, Mar. 2011.

[20] Z. Li, Z. Du, M. Takahashi, K. Saito, and K. Ito, "Reducing mutual coupling of MIMO antennas with parasitic elements for mobile terminals," *IEEE Trans. Antennas Propag.*, vol. 60, no. 2, pp. 473-481, Feb. 2012.

[21] Z. Chen, M. Li, G. Liu, Z. Wu, and M.-C. Tang, "Isolation enhancement for wideband, circularly/dual-polarized, high-density patch arrays using planar parasitic resonators," *IEEE Access*, vol. 7, pp. 112249-112257, Aug. 2019.

[22] J. Li, S. Yang, Y. Gou, J. Hu, and Z. Nie, "Wideband dual-polarized magnetically coupled patch antenna array with high port isolation," *IEEE Trans. Antennas Propag.*, vol. 64, no. 1, pp. 3872-3875, Jan. 2016.

[23] M. Farahani, J. Pourahmadazar, M. Akbari, M. Nedil, A. Sebak, and T. A. Denidni, "Mutual coupling reduction in millimeter-wave MIMO antenna array using a metamaterial polarization-rotator wall," *IEEE Antennas Wirel. Propag. Lett.*, vol. 16, pp. 2324-2327, 2017.

[24] K.-L. Wu, C. Wei, X. Mei, and Z.-Y. Zhang, "Array-antenna decoupling surface," *IEEE Trans. Antennas Propag.*, vol. 65, no. 12, pp. 6728-6738, Dec. 2017.

[25] Z. Niu, H. Zhang, Q. Chen, and T. Zhong, "Isolation enhancement in closely coupled dual-band MIMO patch antennas," *IEEE Antennas Wirel. Propag. Lett.*, vol. 18, no. 8, pp. 1686-1690, 2019.

[26] T. Hassan, M. U. Khan, H. Attia, and M. S. Sharawi, "An FSS based correlation reduction technique for MIMO antennas," *IEEE Trans. Antennas Propag.*, vol. 66, no. 9, pp. 4900-4905, Sep. 2018.

[27] M. Akbari, M.M. Ali, M. Farahani, A.R. Sebak and T. Denidni, "Spatially mutual coupling reduction between CP-MIMO antennas using FSS superstrate," *Electron. Lett.*, vol. 53, no. 8, pp. 516–518, Apr. 2017.

[28] F.-M. Yang, L. Peng, X. Liao, K.-S. Mo, X. Jiang, and S.-M. Li, "Coupling reduction for a wideband circularly polarized conformal array antenna with a single-negative structure," *IEEE Antennas Wirel. Propag. Lett.*, vol. 18, no. 5, pp. 991-995, May 2019.

[29] I. Adam, M. Yasin, N. Ramli, M. Jusoh, H. A. Rahim, T. Latef, T. Izam, and T. Sabapathy, "Mutual coupling reduction of a wideband circularly polarized microstrip MIMO antenna," *IEEE Access*, vol. 7, pp. 97838-97845, Aug. 2019.

[30] J. Zhang, J. Li, and J. Chen, "Mutual coupling reduction of a circularly polarized four-element antenna array using metamaterial absorber for unmanned vehicles," *IEEE Access*, vol. 7, pp. 57469-57475, May 2019.

[31] K. Wei and B.-C. Zhu, "The novel W parasitic strip for the circularly polarized microstrip antennas design and the mutual coupling reduction between them," *IEEE Trans. Antennas Propag.*, vol. 67, no. 2, pp. 804-813, Feb. 2019.

[32] ANSYS/ANSOFT High Frequency Structure Simulation (HFSS), ver. 17.0, ANSYS Corp. [Online]. Available at www.ansoft.com.

[33] D. Zarifi, M. Soleimani, and V. Nayyeri, "Dual- and multiband chiral metamaterial structures with strong optical activity and negative refraction index," *IEEE Antennas Wirel. Propag. Lett.*, vol. 11, pp. 334-337, 2012.

[34] K. Song, Y. Liu, Q. Fu, X. Zhao, C. Luo, and W. Zhu, "90° polarization rotator with rotation angle independent of substrate permittivity and incident angles using a composite chiral metamaterial," *Opt. Express*, vol. 21, no. 6, pp. 7439-7446, Mar. 2013.

[35] R.Jie, H. Jing, S. Li, and Y. Xiao, "Dual-band circular polarizers based on a planar chiral metamaterial structure," *IEEE Antennas Wireless Propag. Lett.,* vol. 18, pp. 2587-2591, 2019.

[36] Y. Liu, K. Song, Y. Qi, S. Gu, and X. Zhao, "Investigation of circularly

polarized patch antenna with chiral metamaterial," *IEEE Antennas Wireless Propag. Lett.,* vol. 12, pp. 1359-1362, 2013.
[37] R. Natarajan, M.Kanagasabai, S.Baisakhiya, R.Sivasamy, S.Palaniswamy, and J. Pakkathillam, "A compact frequency selective surface with stable response for WLAN applications," *IEEE Antennas Wireless Propag. Lett.,* vol. 12, pp. 718-720, 2013.
[38] S. Narayan, G. Gulati, B. Sangeetha, and R. U. Nair, "Novel metamaterial-element-based FSS for airborne radome applications," *IEEE Trans. Antennas Propag.*, vol. 66, no. 9, pp. 4695-4707, Sep. 2018.
[39] X. Zhang, D. Zhang, Y. Fu, S. Li, Y. Wei, K. Chen, X. Wang, and S. Zhuang, "3-D printed swastika-shaped ultrabroadband water-based microwave absorber," *IEEE Antennas Wireless Propag. Lett.,* vol. 19, pp. 821-825, 2020.
[40] A. K. Sarma, H. Arun, M.Kanagasabai, S.Velan, C.Raviteja, and M. Alsath, "Polarisation diverse multiple input–multiple output antenna with enhanced isolation," *IET Microw. Antennas Propag*., vol. 9, no. 12, pp. 1267 - 1273, 2015.

Zhiyuan Chen (S'16) received the B.S. degree in electronic science and technology from the Shandong Normal University (SDNU), Jinan, China, in 2015. He is currently pursuing the Ph.D. degree in electronics and communication engineering with with the School of Microelectronics Communication Engineering, Chongqing University, Chongqing, China.

His current research interests include ultra-wideband antennas, planar antennas and arrays.

Ming-Chun Tang (S'12–M'13–SM'16) received the B. S. degree in physics from the Neijiang Normal University, Neijiang, China, in 2005 and the Ph. D. degree in radio physics from the University of Electronic Science and Technology of China (UESTC), in 2013. From August 2011 to August 2012, he was also with the Department of Electrical and Computer Engineering, The University of Arizona, Tucson, AZ, USA, as a Visiting Scholar. He is currently a full Professor in the School of Microelectronics and Communication Engineering, Chongqing University, China. His research interests include electrically small antennas, RF circuits, metamaterial designs and their applications.

Prof. Tang is the Senior Member of the Chinese Institute of Electronics. He was a recipient of the National Science Fund for Excellent Young Scholars in 2019. He was a recipient of the Best Student Paper Award in the 2010 International Symposium on Signals, Systems and Electronics (ISSSE2010) held in Nanjing, China. His Ph.D. students received Best Student Paper Awards from the IEEE 7th Asia-Pacific Conference on Antennas and Propagation (2018 IEEE APCAP) held in Auckland, New Zealand, 2019 IEEE International Applied Computational Electromagnetics Society (ACES) Symposium held in Nanjing, China, 2019 IEEE International Workshop on Electromagnetics: Applications and Student Innovation Competition held in Qingdao, China, and 2019 Cross Strait Quad-Regional Radio Science and Wireless Technology Conference held in Taiyuan, China. He is the founding Chair of the IEEE AP-S / MTT-S Joint Chongqing Chapter. He serves on the Editorial Boards of several journals, including *IEEE Access*, *Electronics Letters* and *IET Microwaves, Antennas & Propagation*. He has also served on the review boards of various technical journals, and many international conferences as a General Chair, TPC Member, Session Organizer, and the Session Chair.

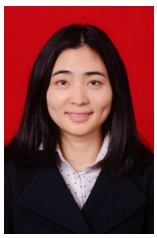

Mei Li (S'15-M'16) received the B.S. degree in electronic information science and technology from the Chengdu University of Information Technology, Chengdu, China, in 2010, and the Ph.D. degree in radio physics from the University of Electronic Science and Technology of China, Chengdu, in 2016. From 2014 to 2016, she was with the Applied Electromagnetics Research Group, University of California at San Diego, San Diego, CA, USA, as a Visiting Graduate. She is currently an Associate Professor in the School of Microelectronics and Communication Engineering, Chongqing University, China.

Her research interests include metasurfaces, antennas and arrays.

Da Yi (S'15 – M' 19) received the B. S. degree and Ph. D. degree in electronic science and technology from Zhejiang University in 2014 and 2019, respectively. He currently works in Chongqing University, Chongqing, China as a tenure-track assistant professor.

Dr. Yi was the recipient of the awards in several international conferences, including Best Student Paper award in the 4th IEEE MTT-S International Wireless Symposium (IWS 2016) and 12th International Workshop on the Electromagnetic Compatibility of Integrated Circuits (EMC COMPO 2019), Best Paper award in the 6th International Symposium on Electromagnetic Compatibility (ISEMC 2019), and the Young Investigator Training Program (YITP) award in the 21st IEEE Workshop on Signal and Power Integrity (SPI 2017). His current research interest is the interference decoupling and noise suppression in antenna arrays and high-speed circuits.

Dongmei Mu, MEng, PhD Candidate, received her bachelor and Master degree from Beijing University of Posts and Telecommunications in 2009 and 2012, respectively.

She is now working as an engineer in Institute of Wireless Mobile Information Technology, School of Electronic Engineering of Beijing University of Posts and Telecommunications. Her research interests are electromagnetic wave propagation and microwave circuits, antenna and switch array. She was awarded the prize of scientific and technological progress from China Institute of Electronics in 2017 and got Excellent Services Award from China Institute of Electronics in 2019.

Richard W. Ziolkowski (M'87–SM'91–F'94-LF'20) received the Sc. B. (*magna cum laude*) degree (Hons.) in physics from Brown University, Providence, RI, USA, in 1974; the M.S. and Ph.D. degrees in physics from the University of Illinois at Urbana-Champaign, Urbana, IL, USA, in 1975 and 1980, respectively; and an Honorary Doctorate degree, *Doctor Technish Honoris Causa*, from the Technical University of Denmark (DTU), Kongens Lyngby, Denmark in 2012.

He is a Distinguished Professor in the Global Big Data Technologies Centre in the Faculty of Engineering and Information Technologies (FEIT) at the University of Technology Sydney, Ultimo NSW Australia. He became a Professor Emeritus at the University of Arizona in 2018, where he was a Litton Industries John M. Leonis Distinguished Professor in the Department of Electrical and Computer Engineering in the College of Engineering and also a Professor in the College of Optical Sciences. He was the Computational Electronics and Electromagnetics Thrust Area Leader with the Engineering Research Division of the Lawrence Livermore National Laboratory, Livermore, CA, USA, before joining The University of Arizona, Tucson, AZ, USA, in 1990. His current research interests include the application of new mathematical and numerical methods to linear and nonlinear problems dealing with the interaction of electromagnetic and acoustic waves with complex linear and nonlinear media, as well as metamaterials, metamaterial-inspired structures, nano-structures, and other classical and quantum applications-specific configurations.

Prof. Ziolkowski was the recipient of the 2019 IEEE Electromagnetics Award (IEEE Technical Field Award). He became a Fellow of the Optical Society of America (OSA) in 2006 and the American Physical Society (APS) in 2016. He was the 2014-2015 Australian DSTO Fulbright Distinguished Chair in Advanced Science and Technology. He served as the President of the IEEE Antennas and Propagation Society (AP-S) in 2005 and has had many other AP-S leadership roles. He is also actively involved with the International Union of Radio Science (URSI), the European Association on Antennas and Propagation (EurAAP), and the International Society for Optics and Photonics (SPIE) professional societies.